Voigt Exceptional Points in an Anisotropic ZnO-Based Planar Microcavity: Square-Root Topology, Polarization Vortices, and Circularity

Steffen Richter, Heinrich-Gregor Zirnstein, Jesús Zúñiga-Pérez, Evgeny Krüger, Christiane Deparis, Lukas Trefflich, Chris Sturm, Bernd Rosenow, Marius Grundmann, Rüdiger Schmidt-Grund

Voigt exceptional-points in an anisotropic ZnO-based planar microcavity: square-root topology, polarization vortices, and circularity

Steffen Richter,[1,2,*] Heinrich-Gregor Zirnstein,[3] Jesús Zúñiga-Pérez,[4] Evgeny Krüger,[1] Christiane Deparis,[4] Lukas Trefflich,[1] Chris Sturm,[1] Bernd Rosenow,[3] Marius Grundmann,[1] and Rüdiger Schmidt-Grund[1,5]

[1] *Universität Leipzig, Felix-Bloch-Institut für Festkörperphysik, Linnéstr. 5, 04103 Leipzig, Germany*
[2] *ELI Beamlines/Fyzikální ústav AV ČR, v.v.i., Za Radnicí 835, 25241 Dolní Břežany, Czech Republic*
[3] *Universität Leipzig, Institut für Theoretische Physik, Brüderstr. 16, 04103 Leipzig, Germany*
[4] *Université Côte d'Azur, CRHEA-CNRS, rue Bernard Grégory, Valbonne, France*
[5] *Technische Universität Ilmenau, Institut für Physik, Weimarer Str. 32, 98693 Ilmenau, Germany*

(Dated: August 2019)

Voigt points represent propagation directions in anisotropic crystals along which optical modes degenerate, leading to a single circularly polarized eigenmode. They are a particular class of exceptional points. Here, we report the fabrication and characterization of a dielectric, anisotropic optical microcavity based on nonpolar ZnO that implements a non-Hermitian system and mimicks the behavior of Voigt points in natural crystals. We prove the exceptional-point nature by monitoring the complex-square-root topology of the mode eigenenergies (real and imaginary parts) around the Voigt points. Polarization state analysis shows, that these artificially engineered Voigt points behave as vortex cores for the linear polarization and sustain chiral modes. Our findings apply to any planar microcavity with broken cylindrical symmetry and, thus, pave the way to exploiting exceptional points in widespread optoelectronic devices as VCSELs and RCLEDs.

The search for topologically non-trivial, photonic systems [1–5] has raised interest in exceptional points (EPs), i.e. non-Hermitian degeneracies of complex-valued eigenenergies that represent topological charges [6–11]. Such branching points have been found in the eigenmodes of various optical resonators [12–18]. A special kind of EPs in optical systems is associated with propagation of circularly polarized light, earlier known as Voigt waves [19]. One key requirement for such EPs is optical biaxiality. It can be established by anisotropic materials in planar microcavities, which are essential building blocks in optoelectronic technology (e.g. VCSELs).

In anisotropic crystals, optical mode degeneracies are connected to different types of singularities, depending on whether the material is transparent or absorptive: In transparent biaxial media, classic optic axes are diabolical points in momentum space, known as Dirac or Hamilton points [20]. The mode dispersion displays a conical intersection that in turn leads to conical refraction [21–23]. If biaxial materials are absorbing, classic optic axes split into pairs of singular optic axes [24, 25]. For propagation along them, the eigenspace of optical modes becomes one-dimensional, allowing only either right or left circularly polarized wavefronts to travel without change of polarization. Only for these directions both, real (refractive index) and imaginary (extinction coefficient) part of the propagation constants degenerate simultaneously. Thus, singular optic axes are EPs in momentum space. Analogously to the diabolical Hamilton points, we term them Voigt points, going back to their discovery by Woldemar Voigt in 1902 [26, 27]. With circularly polarized eigenmodes, Voigt points are an elegant demonstration of chirality which is a fingerprint of EPs [16, 28, 29]. We note that the second requirement for the natural occurrence of Voigt EPs, besides the optical biaxiality, is the presence of (polarization-dependent) absorption.

Bulk absorption (or gain) are intrinsic material properties and hard to modify. To circumvent this limitation

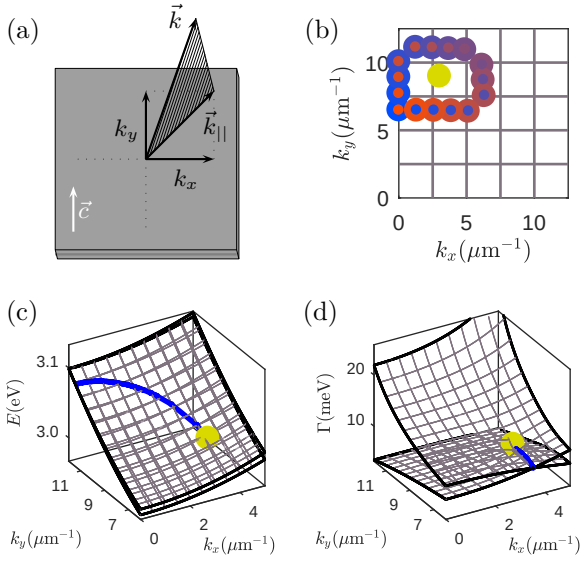

FIG. 1. (a): Sketch of the planar microcavity and coordinates of the in-plane wave-vector $\vec{k}_{||}$ related to the detected light. The material's optic axis ($\vec{c}$) is aligned with the y direction. (b): Schematic position of one Voigt point in the first $\vec{k}_{||}$-quadrant (yellow dot), and trajectory for encirclement (blue-to-red dots, cf. Fig. 4). (c,d): Schematic shape of the complex-energy surface of the modes near this Voigt point (yellow sphere), illustrating the complex-square-root topology. Blue lines mark trajectories of degenerate energy $E_{1,2}$ and broadening $\Gamma_{1,2}$ which overlap only at Voigt points.

we consider a conventional planar microcavity and count on the dissipation caused by photon loss rather than material absorption. The design degrees of freedom (e.g. mirror reflectivities, cavity and mirrors' central wavelengths, etc.) allow a planar microcavity of fully transparent, anisotropic materials to display Voigt points readily accessible within the vacuum light cone [15]. In this letter, we report the fabrication and optical characterization of such a system based on m-plane oriented ZnO. We have measured Stokes vector spectra in the entire two-dimensional momentum space ($\vec{k}_\parallel$, Fig. 1 (a)) of the cavity photon modes and determined their complex-energy dispersion by modeling them with an effective Hamiltonian. We prove simultaneously the complex-square-root topology of the energy surface of the eigenmodes, the generation of linear-polarization vortices, and the correlation between Voigt points and circular polarization.

THEORETICAL CONSIDERATIONS

Light may interfere constructively in a microcavity if its wavelength is commensurable with the effective optical thickness of the cavity layer, giving rise to standing waves (eigenmodes). We first consider a hypothetical anisotropic microcavity without losses. The two polarization-dependent resonance energies of a cavity mode are given by the eigenvalues of a real-valued, Hermitian 2×2 Hamiltonian $\hat{H}_0$:

$$\hat{H}_0 = E_0\hat{1} + A\hat{\sigma}_x + B\hat{\sigma}_z\,, \tag{1}$$

where E_0 is the mean mode energy, A expresses polarization mixing due to the anisotropy of the cavity material (if $k_x, k_y \neq 0$, cf. Fig. 1 (a)) and B reflects the energetic mode splitting due to different, polarization-dependent dispersions. $\hat{1}$ and $\hat{\sigma}_{x,z}$ denote the unit matrix and Pauli spin matrices, respectively. Since the optical thickness of the cavity depends on the propagation angle, the Hamiltonian and its coefficients are functions of the in-plane wave-vector $\vec{k}_\parallel = (k_x, k_y)$. Parallel to the material's optic axis ($k_x = 0$), the modes are purely TE and TM-polarized ($A = 0$). For our cavity configuration, the mode energies become degenerate at $k_y = \pm k_y^0$ [15]. These are two diabolical points which occur at opposite in-plane momenta due to the orthorhombic symmetry of the microcavity. Near them, a linear expansion gives $A \propto k_x$, $B \propto |k_y| - |k_y^0|$ and $E_0 \propto |k_y|$. Thus, they are type-II Dirac points [30].

A real microcavity is leaky and the cavity modes couple to the outside. Using the Mahaux-Weidenmüller formula [31], this can be described by a 2×4 matrix $\hat{W}$ which couples four incoming field components (TE- and TM- polarization on top and bottom side of the microcavity) to the two modes. Effectively, the modes turn into resonances with complex-valued eigenenergies $\tilde{E}_{1,2} = E_{1,2} - i\Gamma_{1,2}$ whose imaginary part describes the exponential decay of the electromagnetic field of a mode. The mode energies are the eigenvalues of the non-Hermitian Hamiltonian $\hat{H} = \hat{H}_0 - i\hat{W}\hat{W}^\dagger$. For a microcavity that is symmetric under reflection along the z-axis, we can decompose $\hat{W} = (\hat{w}\,\hat{w})$ with a 2×2 matrix $\hat{w}$, where

$$\hat{w} = \sqrt{\frac{1}{2}} \begin{pmatrix} \sqrt{\Gamma_0 - C} & 0 \\ 0 & \sqrt{\Gamma_0 + C} \end{pmatrix} \begin{pmatrix} u & -v^* \\ v & u^* \end{pmatrix}\,, \tag{2}$$

with real-valued parameters Γ_0, C with $\Gamma_0 \geq |C|$, and $u, v \in \mathbb{C}$ with $|u|^2 + |v|^2 = 1$. Γ_0 is mean mode broadening (photon loss) and C indicates the polarization-dependence of the loss. To lowest order near the mode degeneracies, Γ_0 and C are constant. The transformation matrix described by u and v allows adjusting the polarization (see below). Consequently, it holds

$$\hat{H} = \hat{H}_0 - i\Gamma_0\hat{1} + iC\hat{\sigma}_z\,. \tag{3}$$

The eigenvalues are

$$\tilde{E}_{1,2} = E_0 - i\Gamma_0 \pm \sqrt{A^2 + (B + iC)^2}. \tag{4}$$

They coincide, $\tilde{E}_1 = \tilde{E}_2$, when $B = 0$ and $|C| = |A|$. In linear approximation near a diabolical point of $\hat{H}_0$, we find this fulfilled at $k_x = k_x^0 \propto \pm C$, $k_y = k_y^0$. These locations are EPs where the Hamiltonian $\hat{H}$ has degenerate eigenvalues, but cannot be diagonalized. Thus, a polarization-dependent loss $C \neq 0$, due to the optical anisotropy of the microcavity, will cause each diabolical point to split into a pair of EPs. They are connected by a curve of coinciding real parts, $E_1 = E_2$, characterized by $B = 0$ and $|A| < |C|$ (cf. blue line in Fig. 1 (c)). The pairs of EPs are connected by a curve with coinciding imaginary part, $\Gamma_1 = \Gamma_2$, where $B = 0$ and $|A| > |C|$ (blue line in Fig. 1 (d)). The characteristic feature of an EP is the square-root topology of the complex eigenvalue surface [6, 32]: When varying the wave vector $\vec{k}_\parallel$ in order to encircle an EP once, continuously following the first mode $\tilde{E}_1(\vec{k}_\parallel)$ will end up in the second mode $\tilde{E}_2$ when the loop returns to its starting point, thus exchanging the modes.

The link between the effective non-Hermitian Hamiltonian (3) and experimentally measured optical spectra is provided by the Mahaux-Weidenmüller formula [31]. For a microcavity that is symmetric under reflection along the z-axis, the reflection Jones matrix is given as

$$\hat{J}(E) = \hat{1} - 2i\hat{w}^\dagger(E\hat{1} - \hat{H})^{-1}\hat{w}\,. \tag{5}$$

In the experiment, we measured the energy-resolved Stokes vector when unpolarized light was reflected from the microcavity. From Eq. (5) we can directly compute the Müller matrix as a function of photon energy E. Its first column corresponds to the Stokes vector from the experiment. Strictly speaking, the above form of the Jones

matrix requires a specific choice of the polarization basis for the incoming light. But we can ignore this in our case, since we illuminate the microcavity with completely unpolarized light. The Hamiltonian Eq. (3) depending on the real-valued parameters A, B, C, E_0, Γ_0 is the most general way to express a 2×2 matrix up to a unitary basis change. A complementary parametrization of the coupling matrix $\hat{w}$ by parameters u and v (Eq. (2)) controls the polarization of the outgoing light. See also supplemental material (SM) [33].

EXPERIMENTAL APPROACH

We have fabricated an anisotropic ZnO-based planar microcavity: First, a 16× $ZnO/Mg_{0.29}Zn_{0.71}O$ distributed Bragg reflector (DBR) and the ZnO cavity layer have been grown on m-plane oriented ZnO substrate by molecular-beam epitaxy [34]. The optical thickness of the cavity layer corresponds to 9/8 of the central wavelength of the DBR (≈ 400 nm), as previous numerical computations indicated this detuning well suitable for the observation of well-separated Voigt points [15, 35]. All ZnO and $Mg_{0.29}Zn_{0.71}O$ layers are m-plane oriented and reveal interface roughnesses below 1 nm [34]. The top-DBR was prepared non-epitaxially by pulsed laser deposition and consists of 6 pairs Al_2O_3 and YSZ (Y-stabilized ZrO_2), all layers being optically isotropic [36]. While the top and bottom DBR are made from different materials, we have matched their reflectivities. The microcavity can be regarded as approximately mirror-symmetric along the vertical axis. All materials are transparent in the energy range of the cavity photon modes (3 eV).

We applied polarization-resolved reflection experiments depending on the angle of incidence θ (10-75° from the surface normal) and sample azimuth angle ϕ (0-360°). Almost 700 configurations (θ, ϕ) were used to map the momentum space of the radiative cavity modes; see Fig. 3. Unpolarized white light from a Xe lamp was reflected off the sample and the Stokes vector $\vec{S} = (S_0, S_1, S_2, S_3)$ obtained [37]. S_0 represents unpolarized reflectance. S_1, S_2 and S_3 are the intensity I differences between the light linearly polarized parallel to x and y, linearly polarized +45° and −45° versus x, and right- and left-circularly polarized, respectively. For each configuration (θ, ϕ), the four Stokes parameter spectra $\vec{S}(E)$ have been modeled simultaneously in a spectral range of 100 meV around the cavity modes. See SM [33] for further details. Measuring the polarization allows us to discriminate both modes even when they overlap in the total intensity $S_0(E)$. Exemplary spectra are shown in Fig. 2 and in the SM [33].

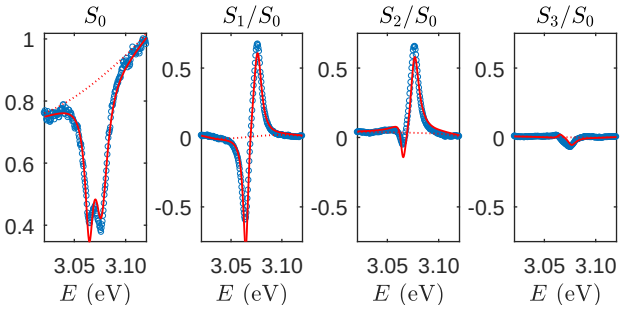

FIG. 2. Representative experimental data (blue dots) and modeling according to Eq. (5) (solid red lines) of normalized Stokes vector spectra $\vec{S}(E)$ at $\vec{k}_\parallel \approx (6.4\,\mu m^{-1}, -6.4\,\mu m^{-1})$, not far from a Voigt point. Dashed red lines represent the baselines. No positive S_3/S_0 occurs.

RESULTS AND DISCUSSION

The eigenvalues of the fitted Hamiltonian are shown in Fig. 3 for the entire momentum space ($\vec{k}_\parallel$); their differences (Fig. 3 (c,f)) reveal the locations where degeneracy of either the mode energies ($\Delta E = 0$) or broadenings ($\Delta\Gamma = 0$) occurs. Four Voigt points are found at approximately $(\pm k_x, \pm k_y) \approx (\pm 4\,\mu m^{-1}, \pm 8\,\mu m^{-1})$. These experimental positions agree with theoretical computations (see Fig. A12 (m-r) in [33]). Figure 3 is already hinting at the complex-square-root topology: While E_1 and E_2 increase continuously with increasing $|\vec{k}_\parallel|$ in any direction, Γ_1 and Γ_2 are discontinuous along k_y. This is the result of sorting the modes such that $E_1 \leq E_2$: the modes are exchanged upon degeneracy ($E_1 = E_2$). Resorting the modes to resolve the discontinuity in $\Gamma_{1,2}$ would result in a discontinuity for $E_{1,2}$ along $\Delta\Gamma = 0$.

To verify the complex-square-root topology of the mode-energy surface, we encircle the EPs in momentum space [12, 38, 39]. See Fig. 4; the path and colors refer to Fig. 1 (b), going clock-wise, starting and finishing at $\vec{k}_\parallel \approx (0\,\mu m^{-1}, 6\,\mu m^{-1})$. One roundtrip in momentum space yields a continuous exchange of the two modes, i.e. the energetically higher (and spectrally narrower) mode becomes the energetically lower (and broader) one and vice versa. Only encircling the Voigt point twice restores the initial situation. As discussed above, another proof for the existence of EPs is parameter C being non-zero while $E_1 = E_2$. Indeed, we obtain values on the order of -3 meV between the Voigt points (see SM [33]).

Once the EP character of the Voigt points has been proven, we analyze their light polarization. Figure 2 shows that only one circular polarization of the reflected light is detected in the vicinity of a Voigt point ($S_3(E)$) although the linear polarization is still opposite for the two modes ($S_{1,2}(E)$). Opposite linear polarizations are expected as long as a Voigt point is not exactly met. Figure 5 depicts the polarization patterns in momentum space. It shows the measured Stokes vector values at energies corresponding to the real part of the mode obtained energies (Fig. 3 (a,b)). The $\vec{k}_\parallel$-dependencies of

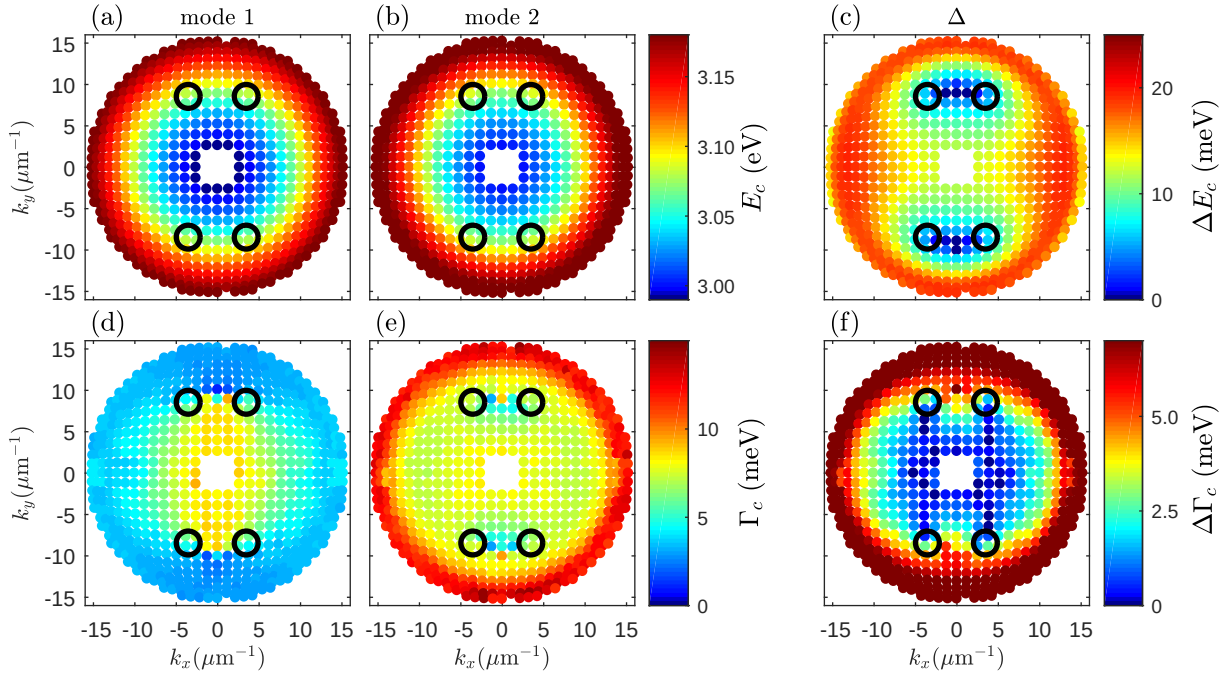

FIG. 3. Complex mode energies $\tilde{E}_{1,2} = E_{1,2} - i\Gamma_{1,2}$ depending on the in-plane wave-vector $\vec{k}_\parallel$ from fitting the Hamiltonian. (a,b): mode energies $E_{1,2}$, (c): their difference $\Delta E = |E_2 - E_1|$. (d,e): mode broadening $\Gamma_{1,2}$, (f): their differences $\Delta\Gamma = |\Gamma_2 - \Gamma_1|$. The positions of the four Voigt points are marked by black circles. Only here, both ΔE and $\Delta\Gamma$ vanish simultaneously. Modes are sorted such that $E_1 \leq E_2$. For comparison, theoretical expectations from numerical computations are shown in Fig. A12 (o,r) in the SM [33].

S_1/S_0 and S_2/S_0 display vortices for the linear polarization: When encircling a pair of Voigt points, the linear polarization changes to the opposite and back. Hence, the pair is a vortex center with winding number 1. As expected, S_1/S_0 is discontinuous along k_y when $\Delta E = 0$ [15]. The experimentally determined degree of circular polarization (S_3/S_0), however, hardly exceeds 10%. Slightly higher degrees of circular polarization have been observed from the same sample in photoluminescence and transmission experiments [33, 35], which might be related to the discrete $\vec{k}_\parallel$ scan. In principal, a non-symmetric matrix operator could result in EPs representing elliptic polarization [40]. That could be caused e.g. by the substrate of the sample. However, numerical computations with proper account of the substrate show that even in this case circularly polarized EPs can be expected (see SM [33]). The lack of high degrees of circular polarization in the experiment seems to be a common problem for polarization-resolved experimental studies in chiral photonic structures [41] and reflects the high sensitivity of EPs to perturbations in general [42, 43]. Nonetheless, it is clear from the experimental data that the vicinity of a Voigt point is related to circular polarization.

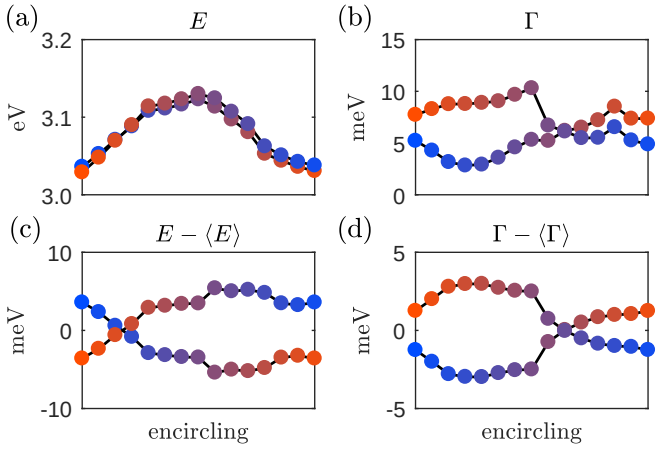

FIG. 4. Clockwise encircling of a Voigt point in $\vec{k}_\parallel$ space along the trajectory shown in Fig. 1 (b) with the same color code. (a): mode energies degenerate near the fourth point; (b): mode broadenings degenerate near the twelfth. Encircling once flips one mode to the other, encircling twice yields the initial situation (complex-square-root topology). For better visibility, the mean values are subtracted in (c,d). See further trajectories in the SM [33].

CONCLUSION

In summary, we have implemented a non-Hermitian model system mimicking a biaxial and absorbing crystal by fabricating an entirely dielectric, planar microcavity with an anisotropic cavity layer (m-plane oriented ZnO).

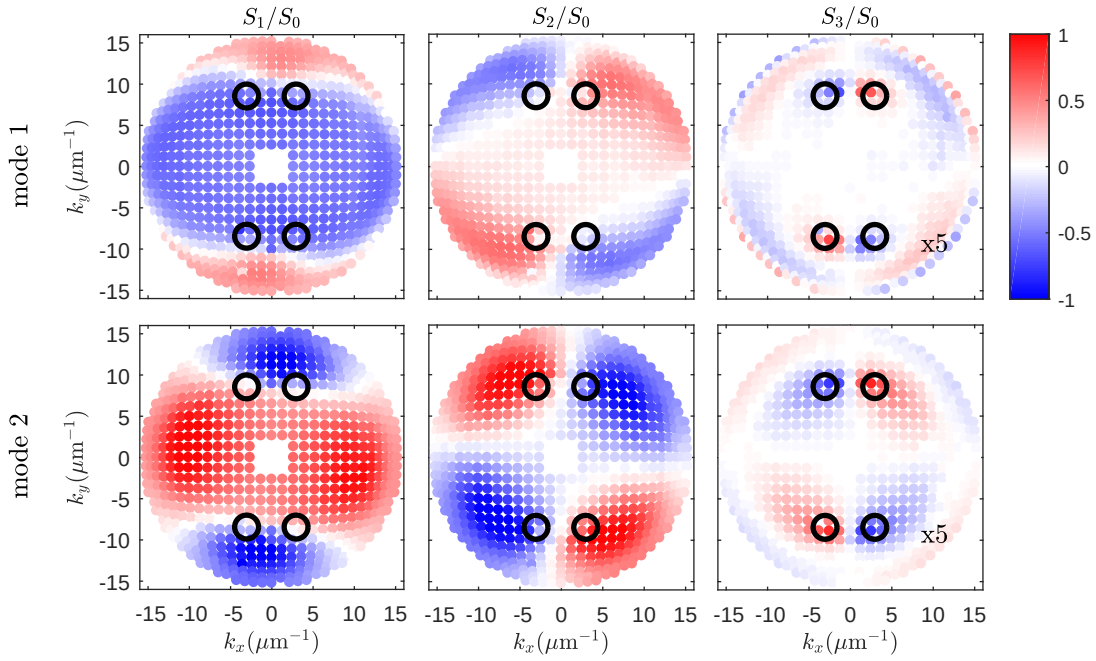

FIG. 5. Measured values of the normalized Stokes vector at the resonance energies obtained from the modeling (Fig. 3 (a,b)). S_3/S_0 is shown 5x enhanced. Approximate positions of the Voigt points are marked by black circles where the circular polarization (S_3) of both modes coincides. See SM, Fig. A13 (c), for comparison with theoretical expectations [33].

Fitting an effective Hamiltonian to our polarization-resolved reflectance data allowed us to obtain the optical mode energies and their degeneracies in the two-dimensional momentum space. We have proven the existence of exceptional points by analyzing the complex-square-root topology of the eigenenergy surface. The measured polarization reveals the circularity of these exceptional points and their role as vortex centers for the linear polarization. We suggest the usage of the term Voigt points for this special kind of exceptional points.

The advantages of our anisotropic microcavity are that i) reliable tracking of the modes upon their exchange is possible thanks to the polarized light spectra, ii) investigating the microcavity under different angular constellations easily allows scanning the relevant parameter space for investigation of the Voigt exceptional points. Finally, it should be noted that our findings apply to any planar microcavity with broken cylindrical symmetry and, thus, pave the way to exploiting exceptional points in widespread optoelectronic devices based on planar microcavities as VCSELs and RCLEDs.

This work was supported by DFG project SCHM 2710/3-1 and by Universität Leipzig in the framework of research profile area Complex Matter. S. R. and H.-G. Z. acknowledge the Leipzig School of Natural Sciences BuildMoNa. H.-G. Z. was funded by DFG SFB 762, L. T. by DFG FOR 1616. We also acknowledge the support of the ANR project "Plug and Bose" (ANR-16-CE24-0021).

* steffen.richter@eli-beams.eu

[1] L. Lu, J. D. Joannopoulos, and M. Soljačić, Nat. Photon. **8**, 821 (2014).
[2] A. B. Khanikaev and G. Shvets, Nat. Photon. **11**, 763 (2017).
[3] J.-X. Zhang, M. C. Rechtsman, and C.-X. Liu, APL Phot. **1**, 050803 (2016).
[4] X.-C. Sun, C. He, X.-P. Liu, M.-H. Lu, S.-N. Zhu, and Y.-F. Chen, Prog. Quantum Electron. **55**, 52 (2017).
[5] Y. Zhang, A. Chen, W. Liu, C. W. Hsu, B. Wang, F. Guan, X. Liu, L. Shi, L. Lu, and J. Zi, Phys. Rev. Lett. **120**, 186103 (2018).
[6] C. Dembowski, H.-D. Gräf, H. L. Harney, A. Heine, W. D. Heiss, H. Rehfeld, and A. Richter, Phys. Rev. Lett. **86**, 787 (2001).
[7] O. Angelsky, A. Mokhun, I. Mokhun, and M. Soskin, Opt. Commun. **207**, 57 (2002).
[8] B. Zhen, C. W. Hsu, Y. Igarashi, L. Lu, I. Kaminer, A. Pick, S.-L. Chua, J. D. Joannopoulos, and M. Soljačic, Nature **525**, 354 (2015).
[9] D. Leykam, K. Y. Bliokh, C. Huang, Y. D. Chong, and F. Nori, Phys. Rev. Lett. **118**, 040401 (2017).
[10] T. Goldzak, A. A. Mailybaev, and N. Moiseyev, Phys. Rev. Lett. **120**, 013901 (2018).
[11] Ş. K. Özdemir, S. Rotter, F. Nori, and L. Yang, Nat. Mater. (2019), 10.1038/s41563-019-0304-9.
[12] C. Dembowski, B. Dietz, H.-D. Gräf, H. L. Harney, A. Heine, W. D. Heiss, and A. Richter, Phys. Rev. E **69**, 056216 (2004).
[13] T. Gao, E. Estrecho, K. Y. Bliokh, T. C. H. Liew, M. D. Fraser, S. Brodbeck, M. Kamp, C. Schneider, S. Höfling,

Y. Yamamoto, F. Nori, Y. S. Kivshar, A. G. Truscott, R. G. Dall, and E. A. Ostrovskaya, Nature **526**, 554 (2015).
[14] B. Peng, Ş. K. Özdemir, M. Liertzer, W. Chen, J. Kramer, H. Yılmaz, J. Wiersig, S. Rotter, and L. Yang, Proc. Nat. Ac. Sci. USA **113**, 6845 (2016).
[15] S. Richter, T. Michalsky, C. Sturm, B. Rosenow, M. Grundmann, and R. Schmidt-Grund, Phys. Rev. A **95**, 023836 (2017).
[16] T. Gao, G. Li, E. Estrecho, T. C. H. Liew, D. Comber-Todd, A. Nalitov, M. Steger, K. West, L. Pfeiffer, D. W. Snoke, A. V. Kavokin, A. G. Truscott, and E. A. Ostrovskaya, Phys. Rev. Lett. **120**, 065301 (2018).
[17] C.-H. Yi, J. Kullig, and J. Wiersig, Phys. Rev. Lett. **120**, 093902 (2018).
[18] J. Zhang, B. Peng, Ş. K. Özdemir, K. Pichler, D. O. Krimer, G. Zhao, F. Nori, Y.-X. Liu, S. Rotter, and L. Yang, Nat. Photon. **12**, 479 (2018).
[19] T. G. Mackay and A. Lakhtakia, J. Opt. A: Pure Appl. Opt. **5**, 91 (2003).
[20] M. V. Berry and M. R. Dennis, Proc. R. Soc. Lond. A **459**, 1261 (2003).
[21] H. Lloyd, Philos. Mag. **2**, 112 (1833).
[22] L. D. Landau and E. M. Lifschitz, *Elektrodynamik der Kontinua*, edited by G. Heber, Lehrbuch der theoretischen Physik, Vol. VIII (Akademie-Verlag).
[23] M. V. Berry and M. R. Jeffrey, "Conical diffraction: Hamilton's diabolical point at the heart of crystal optics," in *Progress in Optics*, Vol. 50, edited by E. Wolf (Elsevier, 2008) Chap. 2, p. 13.
[24] C. Sturm and M. Grundmann, Phys. Rev. A **93**, 053839 (2016).
[25] M. Grundmann, C. Sturm, C. Kranert, S. Richter, R. Schmidt-Grund, C. Deparis, and J. Zúñiga-Pérez, Phys. Status Sol. RRL **11**, 1600295 (2017).
[26] W. Voigt, Philos. Mag. 6, **4**, 90 (1902).
[27] W. Voigt, Götting. Nachr. **1**, 48 (1902).
[28] W. D. Heiss and H. L. Harney, Eur. Phys. Jour. D **17**, 149 (2001).
[29] D. Solnyshkov and G. Malpuech, Comptes Rendus Physique **17**, 920 (2016).
[30] A. A. Soluyanov, D. Gresch, Z. Wang, Q. Wu, M. Troyer, X. Dai, and B. A. Bernevig, Nature **527**, 495 (2015).
[31] C. Mahaux and H. A. Weidenmüeller, *Shell-model approach to nuclear reactions* (North-Holland, 1969).
[32] H. Cao and J. Wiersig, Rev. Mod. Phys. **87**, 61 (2015).
[33] See Supplemental Material at [URL will be inserted by publisher].
[34] J. Zúñiga-Pérez, L. Kappei, C. Deparis, F. Reveret, M. Grundmann, E. de Prado, O. Jamadi, J. Leymarie, S. Chenot, and M. Leroux, Appl. Phys. Lett. **108**, 251904 (2016).
[35] S. Richter, *Optically anisotropic planar microcavities*, Dissertation, Universität Leipzig 2018, http://nbn-resolving.de/urn:nbn:de:bsz:15-qucosa2-208912.
[36] H. Franke, C. Sturm, R. Schmidt-Grund, G. Wagner, and M. Grundmann, New J. Phys. **14**, 013037 (2012).
[37] R. A. Chipman, "Polarimetry," in *Handbook of Optics*, edited by M. Bass (McGraw-Hill, 1995) Chap. 22.
[38] J. Doppler, A. A. Mailybaev, J. Böhm, U. K. andA. Girschik, F. Libisch, T. J. Milburn, P. Rabl, N. Moiseyev, and S. Rotter, Nature **537**, 76 (2016).
[39] A. U. Hassan, B. Zhen, M. Soljačić, M. Khajavikhan, and D. N. Christodoulides, Phys. Rev. Lett. **118**, 093002 (2017).
[40] M. Grundmann, S. Richter, T. Michalsky, C. Sturm, J. Zúñiga-Pérez, and R. Schmidt-Grund, Proc. SPIE **10105**, 101050K (2017).
[41] S. Takahashi, Y. Ota, T. Tajiri, J. Tatebayashi, S. Iwamoto, and Y. Arakawa, Phys. Rev. B **96**, 195404 (2017).
[42] J. Wiersig, Phys. Rev. A **93**, 033809 (2016).
[43] W. Chen, Ş. K. Özdemir, G. Zhao, J. Wiersig, and L. Yang, Nature **548**, 192 (2017).